© 2018. Published by The Company of Biologists Ltd | Development (2018) 145, dev161893. doi:10.1242/dev.161893

RESEARCH ARTICLE

Forced lipophagy reveals that lipid droplets are required for early embryonic development in mouse

Takayuki Tatsumi[1,2,§], Kaori Takayama[3,§], Shunsuke Ishii[4], Atsushi Yamamoto[2,*], Taichi Hara[5], Naojiro Minami[6], Naoyuki Miyasaka[2], Toshiro Kubota[2,‡], Akira Matsuura[3,4,7], Eisuke Itakura[3,4,7,¶] and Satoshi Tsukamoto[1,¶]

ABSTRACT

Although autophagy is classically viewed as a non-selective degradation system, recent studies have revealed that various forms of selective autophagy also play crucial physiological roles. However, the induction of selective autophagy is not well understood. In this study, we established a forced selective autophagy system using a fusion of an autophagy adaptor and a substrate-binding protein. In both mammalian cells and fertilized mouse embryos, efficient forced lipophagy was induced by expression of a fusion of p62 (Sqstm1) and a lipid droplet (LD)-binding domain. In mouse embryos, induction of forced lipophagy caused a reduction in LD size and number, and decreased the triglyceride level throughout embryonic development, resulting in developmental retardation. Furthermore, lipophagy-induced embryos could eliminate excess LDs and were tolerant of lipotoxicity. Thus, by inducing forced lipophagy, expression of the p62 fusion protein generated LD-depleted cells, revealing an unexpected role of LD during preimplantation development.

KEY WORDS: Autophagy, Lipid droplet, Oocyte, Embryo, Mouse

INTRODUCTION

Macroautophagy (hereafter referred to as autophagy) is an evolutionarily conserved system of 'self-eating', in which cytoplasmic content is engulfed by the autophagosome and delivered to the lysosome for degradation (Mizushima, 2007). Although autophagy was originally characterized as a non-selective bulk degradation pathway, recent studies revealed that autophagy plays crucial roles in selective degradation of cellular components, including organelles (Okamoto, 2014; Stolz et al., 2014). Autophagy adaptors, which act as cargo receptors for selective degradation, play important roles in determining selectivity for target organelles. The most well-characterized adaptor is p62 (also known as Sqstm1), which contains an LC3-recognition sequence (LRS)/LC3-interacting region (LIR), a ubiquitin-associated (UBA) domain, and a Phox and Bem1p (PB1) domain, which are responsible for dimerization and multimerization of the protein (Katsuragi et al., 2015). To activate selective autophagy, surface proteins on damaged organelles (e.g. mitochondria) or microbes are first ubiquitylated by ubiquitin ligase. Then, autophagy adaptors, such as p62, are recruited onto the damaged organelle via interactions with the ubiquitylated proteins. The adaptors on the damaged organelle are recognized by LC3 (Map1lc3b), and the target is then engulfed by the autophagosome (Anding and Baehrecke, 2017; Stolz et al., 2014). Therefore, the crucial steps in selective autophagy are recruitment of an adaptor to the substrate and the interaction of the adaptor with LC3.

Lipid droplets (LDs) are unique organelles that store lipids essential for cellular energy (metabolism) and membrane production (Thiam et al., 2013; Walther and Farese, 2012). LDs consist of a neutral lipid core, mainly made up of triglyceride (TG) and cholesterol esters, and are coated by a phospholipid monolayer and various proteins such as the perilipins (Plins) [Plin1, ADRP (Plin2; also known as adipophilin), TIP47 (Plin3), Plin4 (also known as S3-12) and Plin5 (also known as OXPAT)]. The Plins share a conserved sequence, the PAT domain, primarily at the N terminus, which is essential for the LD interaction (Bickel et al., 2009). In mammals, several Plins are widely expressed (e.g. ADRP and TIP47), whereas others are expressed in a tissue-specific manner (e.g. Plin1 in adipocytes and steroidogenic cells) (Bickel et al., 2009). LDs are present in all tissues, and serve various functions in addition to lipid storage (Fujimoto and Parton, 2011).

Lysosomes contain both proteases and acidic lipases. Indeed, LDs are also targets of a form of selective autophagy termed lipophagy. During this process in mammals, yeast and *Caenorhabditis elegans*, LDs are transported to the lysosomes (O'Rourke and Ruvkun, 2013; Singh et al., 2009; Wang et al., 2014), where they are broken down by acidic lipases. This suggests that regulation of lipophagy might provide a therapeutic approach to preventing metabolic syndrome. However, the molecular machinery responsible for lipophagy, including its specific adaptors, remains uncharacterized.

In the mammalian oocyte, a considerable number of LDs accumulate during oogenesis, although the amount differs across species (Sturmey et al., 2009). For example, in comparison with mouse, porcine oocytes contain massive amounts of LDs (Leese, 2012), which interferes with embryonic manipulation, especially in the context of cryopreservation (Nagashima et al., 1995). The physiological function of LDs stored in the oocyte/embryo is species specific, but, in general, LDs are required for energy (i.e. ATP) production during preimplantation embryonic development

[1]Laboratory Animal and Genome Sciences Section, National Institute for Quantum and Radiological Science and Technology, Anagawa, Inage-ku, Chiba 263-8555, Japan. [2]Comprehensive Reproductive Medicine, Regulation of Internal Environment and Reproduction, Graduate School, Tokyo Medical and Dental University, Tokyo 113-8519, Japan. [3]Department of Nanobiology, Graduate School of Advanced Integration Science, Chiba University, Inage-ku, Chiba 263-8522, Japan. [4]Department of Biology, Faculty of Science, Chiba University, Yayoi-cho, Inage-ku, Chiba 263-8522, Japan. [5]Laboratory of Cellular Regulation, Faculty of Human Sciences, Waseda University, Tokorozawa, Saitama 359-1192, Japan. [6]Laboratory of Reproductive Biology, Graduate School of Agriculture, Kyoto University, Kyoto 606-8502, Japan. [7]Department of Biology, Graduate School of Science, Chiba University, Inage-ku, Chiba 263-8522, Japan.
*Present address: Department of Urology, Dokkyo Medical University, Koshigaya Hospital, Saitama 343-8555, Japan. ‡Present address: Tokyo Kyosai Hospital, Nakameguro, Meguro-ku, Tokyo 153-8934, Japan.
§These authors contributed equally to this work

¶Authors for correspondence (eitakura@chiba-u.jp; tsukamoto.satoshi@qst.go.jp)

E.I., 0000-0001-7248-9333; S.T., 0000-0001-7063-8825

Received 29 November 2017; Accepted 23 January 2018

Development (2018) 145, dev161893. doi:10.1242/dev.161893

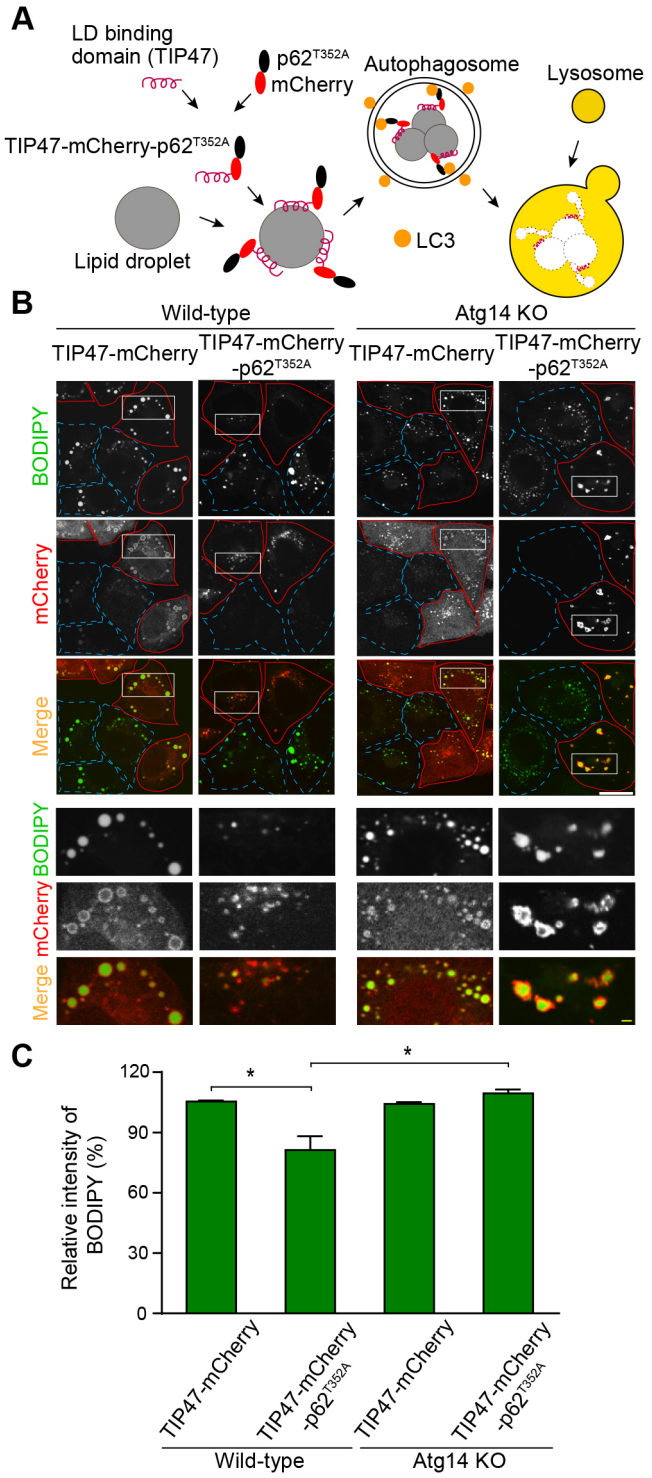

Fig. 1. Forced lipophagy by expression of TIP47-mCherry-p62^{T352A} in cultured mammalian cells. (A) Schematic of forced lipophagy. The LD-binding domain from TIP47 was fused with p62^{T352A} and mCherry. TIP47-mCherry-p62^{T352A} interacts with LC3 on the autophagosomal membrane via the LD-binding domain, and is then incorporated into autophagosomes via the p62–LC3 interaction. TIP47-mCherry-p62^{T352A}-coated LDs were broken down by lysosomal lipases. (B) Wild-type and Atg14 KO HeLa cells expressing TIP47-mCherry or TIP47-mCherry-p62^{T352A} were cultured with OA for 24 h. LDs were stained with BODIPY 493/503 and analyzed by immunofluorescence microscopy. Red and blue dashed lines outline cells expressing or not expressing mCherry-fusion protein, respectively. Bottom panels show higher magnification images of the boxed regions. Scale bars: 10 µm (top panels); 1 µm (bottom panels). (C) Cells expressing TIP47-mCherry or TIP47-mCherry-p62^{T352A} were cultured with OA for 24 h. Then, LDs were stained with BODIPY 493/503, and the total amount of LD per cell was determined by flow cytometry. The relative intensity of BODIPY 493/503 fluorescence in mCherry-positive cells is expressed as a percentage relative to that in mCherry-negative cells. Data represent mean ±s.e.m. *P<0.05. Data are representative of three independent experiments.

(Dunning et al., 2014). LDs stored in the oocyte dynamically change their morphology during oocyte maturation and subsequent embryonic development. In unfertilized (MII) oocytes (before fertilization), LDs are mostly detected as clustered structures, which disperse into smaller droplets soon after fertilization (Bradley et al., 2016; Watanabe et al., 2010). Interestingly, when MII oocytes are cultured without pyruvate and glutamine (i.e. energy-depleted conditions), the clustered LDs are dispersed (Bradley et al., 2016). Thus, LD morphology changes in response to cellular energy level.

In this study, we developed a system of forced lipophagy using a fusion protein of p62 and TIP47, an LD-binding domain. Using this system, we demonstrated that the amount of LDs was decreased upon induction of forced lipophagy in cultured mammalian cells expressing TIP47-p62. Our results demonstrate that maintenance of the proper amount of LDs is important for early embryonic development.

RESULTS

Induction of forced lipophagy in cultured mammalian cells

We hypothesized that expression of an artificial linker protein that connects substrates to the autophagosomal membrane would induce selective autophagy. p62 is a well-characterized adaptor that binds to LC3 via the LIR motif (Ichimura et al., 2008; Pankiv et al., 2007). Given that overexpression of p62 results in Nrf2 (Nfe2l2) activation through Keap1 binding, we used the p62^{T352A} mutant, which lacks the Keap1 interaction (Komatsu et al., 2010). The PAT domain of TIP47 has a high binding affinity for LD surfaces, and efficiently competes with other proteins from LD surface (Bulankina et al., 2009; Kory et al., 2015). Therefore, we fused the PAT domain with p62^{T352A} and the red fluorescent protein mCherry, yielding TIP47-mCherry-p62^{T352A} (Fig. 1A). To determine whether this fusion protein could induce lipophagy, we expressed TIP47-mCherry-p62^{T352A} in HeLa cells and visualized LDs using the fluorescent neutral lipid dye BODIPY 493/503. HeLa cells in regular media contain few LDs, and no significant change in the number of LDs was detected in cells expressing TIP47-mCherry-p62^{T352A} (data not shown). Therefore, to induce high levels of LDs, we treated the cells with oleic acid (OA). In the treated cells, the amount of LDs was markedly decreased by expression of TIP47-mCherry-p62^{T352A} in comparison with TIP47-mCherry (Fig. 1B). To determine whether the reduction of LDs was dependent on autophagic degradation activity, we expressed TIP47-mCherry-p62^{T352A} in Atg14 knockout (KO) cells, which are defective in autophagosome formation (Itakura et al., 2008). The Atg14 KO cells did not exhibit any reduction in the amount of LDs upon expression of TIP47-mCherry-p62^{T352A} (Fig. 1B), suggesting that TIP47-mCherry-p62^{T352A} induced degradation of LDs, but did not inhibit LD synthesis or recruitment of endogenous LD-associated proteins to LDs. Analysis of the fluorescence intensity of BODIPY 493/503 by flow cytometry confirmed that the amount of LDs per cell was lower in OA-treated cells expressing TIP47-mCherry-p62^{T352A} than in mCherry-negative cells (Fig. 1C), indicating that expression of TIP47-mCherry-p62^{T352A} in cells accelerates breakdown of LDs via forced lipophagy.

Development (2018) 145, dev161893. doi:10.1242/dev.161893

Induction of forced lipophagy in fertilized mouse embryos

This finding prompted us to perform a functional analysis of cells in which LDs were depleted by forced lipophagy. For this purpose, we focused on mouse early embryonic development, for several reasons. First, because LDs accumulate during oogenesis, oocytes contain considerable numbers of LDs. Second, autophagy is highly activated after fertilization, and is essential for early embryonic development (Tsukamoto et al., 2008). Third, the physiological function of LDs during embryonic development remains largely unknown. To induce forced lipophagy after fertilization, we microinjected mRNAs encoding either TIP47-mCherry (control) or TIP47-mCherry-p62^{T352A} (lipophagy-induced) into the cytoplasm of one-cell embryos (Fig. 2A). The embryos were collected 4-5 h after *in vitro* fertilization (IVF), the time at which autophagy is highly activated (Tsukamoto et al., 2008). Induction of lipophagy resulted in formation of LD clusters, which were subsequently delivered to the cell periphery during embryonic development. No such clustering and movement of LDs was observed in control embryos (Fig. 2B, Fig. S1A, Movie 1). We confirmed that the clustered LDs observed in lipophagy-induced embryos were specifically labeled with BODIPY 493/503 (Fig. 2C). Similar changes in LD morphology after lipophagy induction occurred in embryos collected from another mouse strain, C3H (Fig. S1B). By contrast, in control embryos, LDs were distributed uniformly, as reported previously (Bradley et al., 2016; Watanabe et al., 2010), although TIP47-mCherry signals failed to localize to the LD surface and were diffused throughout the cytoplasm, probably owing to the abundance of ADRP protein in mouse oocytes and embryos, which could block access of TIP47-mCherry to LDs (see also Fig. S1C,D and Discussion).

In lipophagy-induced embryos, the content of TG, a major component of LDs, decreased approximately 50% at the eight-cell stage in comparison with control embryos (Fig. 2D). Furthermore, quantitative analysis of electron micrographs of the four-cell stage revealed that induction of lipophagy significantly decreased LD number and size (Fig. 2E). Thus, forced lipophagy caused not only morphological changes of LDs, but also a reduction in intracellular lipid storage.

Although we used the p62^{T352A} mutant to prevent secondary effects of p62, we were still concerned that p62 overexpression alone might induce lipophagy, largely because p62 plays multiple roles in cell signaling, including lipid metabolism (Rodriguez et al., 2006). To eliminate this concern, we synthesized mRNA encoding DsRed-p62^{WT} (fusion protein of DsRed and wild-type p62) and microinjected it into one-cell embryos. DsRed-p62^{WT} was detected as cytoplasmic puncta that stained with an anti-ubiquitin antibody that recognizes poly-ubiquitylated proteins, representing protein aggregates, indicating that DsRed-p62^{WT} was functional (Fig. 3A). We also confirmed that these p62-positive foci partially overlapped with LC3 (autophagosome marker) and Lamp1 (lysosome-associated membrane protein 1, a lysosome marker), indicating that, like LC3, overexpressed p62 also functions as an autophagy adaptor (Fig. 3B). Importantly, DsRed-p62^{WT} expression induced neither LD clustering nor a close interaction between DsRed-p62^{WT} and LDs throughout embryonic development (Fig. 3C). Therefore, we concluded that the clustering and movement of LDs observed in lipophagy-induced embryos was unlikely to be due to p62 overexpression, and was instead dependent on p62 localization on the LD surface.

Forced lipophagy depends on autophagy

To determine whether forced lipophagy was autophagy dependent, we first analyzed the localization of clustered LDs relative to autophagosomes and lysosomes. Immunofluorescence analysis revealed that both LC3 (autophagosome) and Lamp1 (lysosome) were in close proximity to the clustered LDs in lipophagy-induced embryos, but not in non-injected control embryos (Fig. 4A,B). In the presence of wortmannin [a phosphoinositide 3-kinase (PI3K) inhibitor, which blocks the initial step of autophagy], this close localization was lost, although the clustered LDs were still present. Furthermore, treatment with chloroquine, an inhibitor of lysosomal hydrolases, not only inhibited LD clustering and association with autophagosomes and lysosomes, but also changed the lysosome positioning: specifically, the predominantly peripheral localization of lysosomes was abolished (Fig. 4A,B).

To further assess the specificity of LD clustering upon autophagy, we microinjected siRNA targeting Atg14 along with mRNAs encoding either TIP47-mCherry or TIP47-mCherry-p62^{T352A}. In these embryos, LC3 dots (representing autophagosomes) were almost absent (Fig. 4C), and embryonic development was impaired, as a result of efficient inhibition of autophagy (Fig. S2A,B). Additionally, LD clustering was diminished, and lysosomal association of LDs was weaker in siRNA-treated lipophagy-induced embryos than in control lipophagy-induced embryos (Fig. 4D, Fig. S2C).

Consistent with our immunofluorescence results, electron microscopic analysis of lipophagy-induced embryos confirmed the abundance of lysosomes and autolysosomes, which were localized proximally to the clustered LDs at the cell periphery (Fig. 4E).

We next investigated whether lipophagy induction would alter endogenous autophagic activity. To this end, we cultured embryos microinjected with either TIP47-mCherry or TIP47-mCherry-p62^{T352A} mRNA in the presence or absence of bafilomycin A_1 ($BafA_1$, a lysosomal inhibitor), and then performed immunoblotting with anti-LC3 antibody. The autophagic flux did not differ significantly between control and lipophagy-induced embryos (Fig. 4F), indicating that endogenous autophagic activity was not altered after induction of lipophagy.

To further assess whether lipophagy induction was autophagy specific, we expressed TIP47-mCherry-p62^{T352A} in unfertilized (MII) oocytes, in which autophagic activity is low, and cultured them for 2 days *in vitro*. Under these conditions, LD clustering occurred, whereas LD translocation did not (Fig. 4G), indicating that p62 expression at the LD surface is responsible for LD clustering even under low (or absent) autophagic activity, whereas high autophagic activity is required for LD movement to the periphery. Taken together, these results suggested that forced lipophagy occurs in an autophagy-dependent manner.

Developmental potential of lipophagy-induced embryos

Based on these results, we hypothesized that lipophagy-induced embryos have higher developmental potential as a result of their more efficient utilization of intracellular LDs in comparison with normal embryos. To investigate this possibility, we cultured embryos microinjected with either TIP47-mCherry or TIP47-mCherry-p62^{T352A} mRNA for 4-5 days *in vitro*. Unexpectedly, the proportion of embryos reaching the late blastocyst stage within this time frame was lower in lipophagy-induced embryos (30.7%) than in control embryos (56.7%) (Fig. 5A,B). Because the mouse embryo is particularly reliant on exogenous nutrients (Leese, 2012), we then cultured control and lipophagy-induced embryos without amino acids. The blastocyst formation rate of the lipophagy-induced embryos was not influenced by the presence or absence of amino acids, whereas amino acid deficiency significantly decreased the

Development (2018) 145, dev161893. doi:10.1242/dev.161893

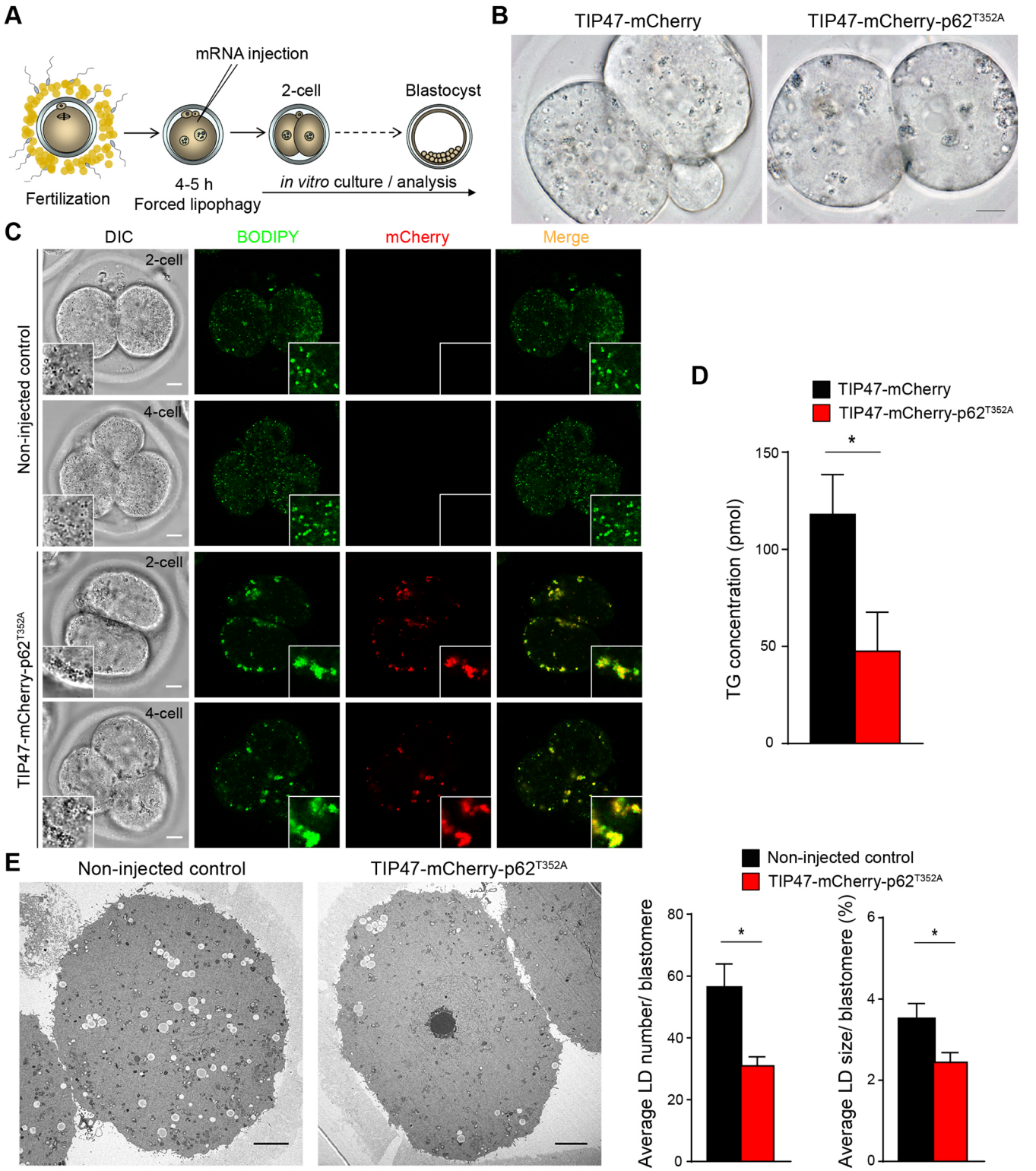

Fig. 2. Forced lipophagy in fertilized mouse embryos. (A) Experimental design for analysis of forced lipophagy during preimplantation embryonic development. To induce lipophagy, TIP47-mCherry-p62^{T352A} mRNA was microinjected into the cytoplasm at the one-cell stage, and the embryos were analyzed. (B) Morphology of LDs in two-cell embryos expressing either TIP47-mCherry or TIP47-mCherry-p62^{T352A}. (C) Embryos microinjected with or without TIP47-mCherry-p62^{T352A} mRNA were stained with BODIPY 493/503 at the indicated stages, and observed by laser confocal fluorescence microscopy. DIC, differential interference contrast. Insets show higher-magnification images. (D) Triglyceride (TG) levels at the eight-cell stage in embryos microinjected with either TIP47-mCherry (control) or TIP47-mCherry-p62^{T352A} mRNA. Data are representative of five independent experiments with 40 embryos per experiment. (E) Electron microscopic analysis of embryos not injected (non-injected control) or injected with TIP47-mCherry-p62^{T352A} mRNA (lipophagy-induced) at the four-cell stage. Right panels: quantification of LD size and number per blastomere in non-injected control (15 blastomeres selected randomly from five embryos) and lipophagy-induced (11 blastomeres selected randomly from four embryos) embryos. Error bars represent s.e.m.; *P<0.05 (Student's t-test). Scale bars: 10 µm (B,C); 5 µm (E).

Development (2018) 145, dev161893. doi:10.1242/dev.161893

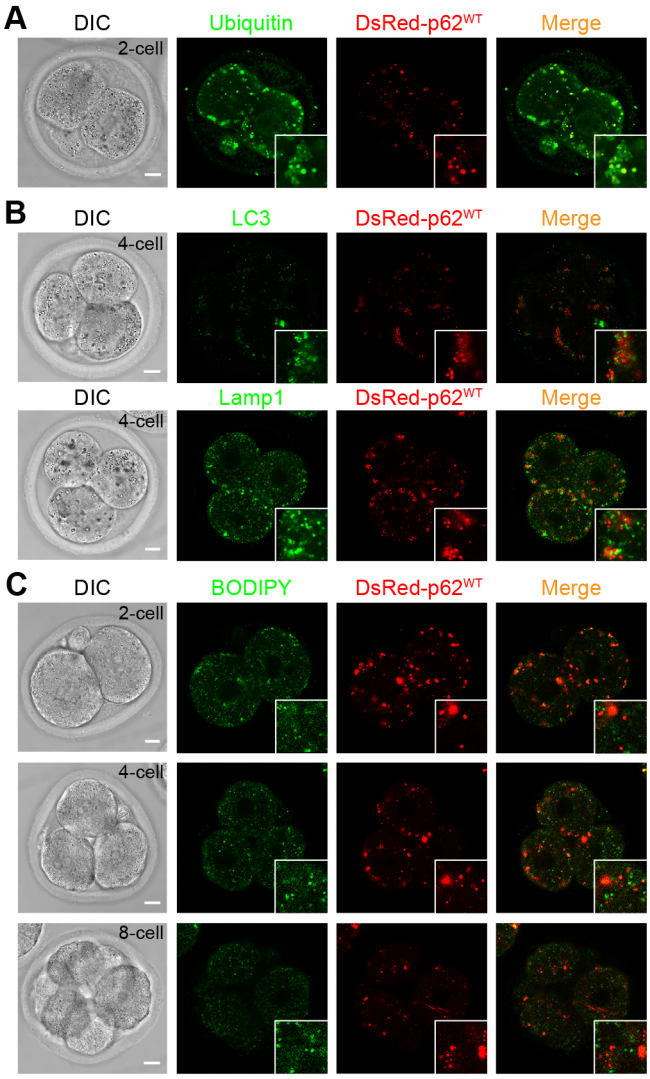

Fig. 3. p62 overexpression does not alter LD morphology. (A) Embryos microinjected with DsRed-p62^{WT} mRNA were cultured to the two-cell stage, stained with anti-ubiquitin antibody and observed by laser confocal fluorescence microscopy. (B) Embryos microinjected with DsRed-p62^{WT} mRNA were cultured to the four-cell stage, stained with anti-LC3 or Lamp1 antibodies, and observed by laser confocal fluorescence microscopy. (C) Embryos microinjected with DsRed-p62^{WT} mRNA were cultured to the indicated stages, stained with BODIPY 493/503, and observed by laser confocal fluorescence microscopy. DIC, differential interference contrast. Insets show higher-magnification images. Scale bars: 10 µm.

rate of development in control embryos (Fig. 5A,B). These results imply that utilization of intracellular LDs is important for early embryogenesis, particularly in the absence of extracellular energy sources.

The intracellular distribution of LDs may be linked to energy balance, e.g. the close association of LDs with mitochondria facilitates ATP production via β-oxidation (Herms et al., 2015). Accordingly, we analyzed the ATP content in lipophagy-induced embryos. Throughout embryonic development, ATP content did not differ significantly between lipophagy-induced and control embryos (Fig. S3A). Consistent with this, clustered LDs were not localized in close proximity to mitochondria in lipophagy-induced embryos (Fig. S3B). In addition, we observed no significant difference in cellular levels of reactive oxygen species (ROS) between control and lipophagy-induced embryos (Fig. S3C). These data indicate that lipophagy induction is not directly involved in increasing cellular ATP, even when mitochondrial function is not impaired.

We further assessed the contribution of lipolysis to lipophagy-induced embryos. To this end, we cultured either control or lipophagy-induced embryos with OA, to stimulate TG synthesis, in the presence or absence of the lipase inhibitor diethylumbelliferyl phosphate (DEUP). OA supplementation had a negative influence on embryonic development in control embryos, but not in lipophagy-induced embryos (Fig. 5A-D, Fig. S4). Moreover, in the presence of DEUP, almost all control embryos were developmentally retarded, probably owing to excess accumulation of LDs, whereas 12.7% of lipophagy-induced embryos survived even to the late blastocyst stage (Fig. 5C,D, Fig. S4).

Palmitic acid (PA, a saturated fatty acid) is more lipotoxic than OA (unsaturated fatty acid) in a variety of cell lines (Listenberger et al., 2003). To assess tolerance of lipotoxicity, we cultured control or lipophagy-induced embryos with PA to the blastocyst stage. PA treatment substantially decreased the developmental rate (i.e. the rate at which the embryos formed blastocysts) in both groups (Fig. 5A,B,E,F), probably as a result of lipotoxicity. However, the level of apoptosis, indicative of lipotoxicity, was lower in the lipophagy-induced embryos than in control embryos (Fig. 5G).

Taken together, these data indicate that forced lipophagy plays an important role in avoiding excess LD accumulation, and can confer resistance to lipotoxicity.

DISCUSSION

In this study, we developed a system for inducing forced selective autophagy of LDs, termed forced lipophagy, using a fusion protein of p62 and an LD-binding domain. p62 on the surface of LDs can be recognized as an autophagic cargo, facilitating the interaction with LC3 through its LC3-interacting region (LIR). LC3 stably binds to the autophagosomal membrane, forming a bridge between LDs and the membrane. The autophagosomal membrane then elongates to form the autophagosome, which encloses a portion of LDs, and subsequently fuses with the lysosome for degradation (see our proposed model, Fig. S5). LDs are also metabolized (i.e. degraded) by cytosolic neutral lipases such as adipose triglyceride lipase (ATGL; PNPLA2) and hormone-sensitive lipase (HSL; LIPE), both of which contain LC3-binding motifs required for their lipolytic activities (Martinez-Lopez et al., 2016). In addition, lipolysis is tightly coupled with chaperone-mediated autophagy (CMA) (Kaushik and Cuervo, 2015). Although additional unknown factor(s) and mechanism(s) such as self-oligomerization of p62 via the PB1 domain (which may promote LD clustering) and degradation of LD coat proteins (Plins) by the proteasome (which may stabilize the association of p62 on the LD surface) might contribute to this process, our results strongly suggest that expression of p62 on the LD surface is sufficient to induce selective LD degradation in mammalian cells and fertilized mouse embryos.

We observed that induction of lipophagy in mouse embryos caused LD clustering and translocation to the cell periphery. This clustering also occurred in cultured mammalian cells, whereas translocation did not (data not shown), suggesting that the latter process is mediated by an embryo-specific mechanism. Although the mechanism underlying this process is not fully understood, lipophagic activity in embryos might be required for subsequent translocation of clustered LDs to the cell periphery. Consistent with this idea, in unfertilized oocytes (in which autophagic activity is low), expression of TIP47-mCherry-p62^{T352A} caused LD clustering but not subsequent movement. Similar results were obtained when lipophagy-induced embryos were cultured with wortmannin, an inhibitor of autophagy, and injected

Development (2018) 145, dev161893. doi:10.1242/dev.161893

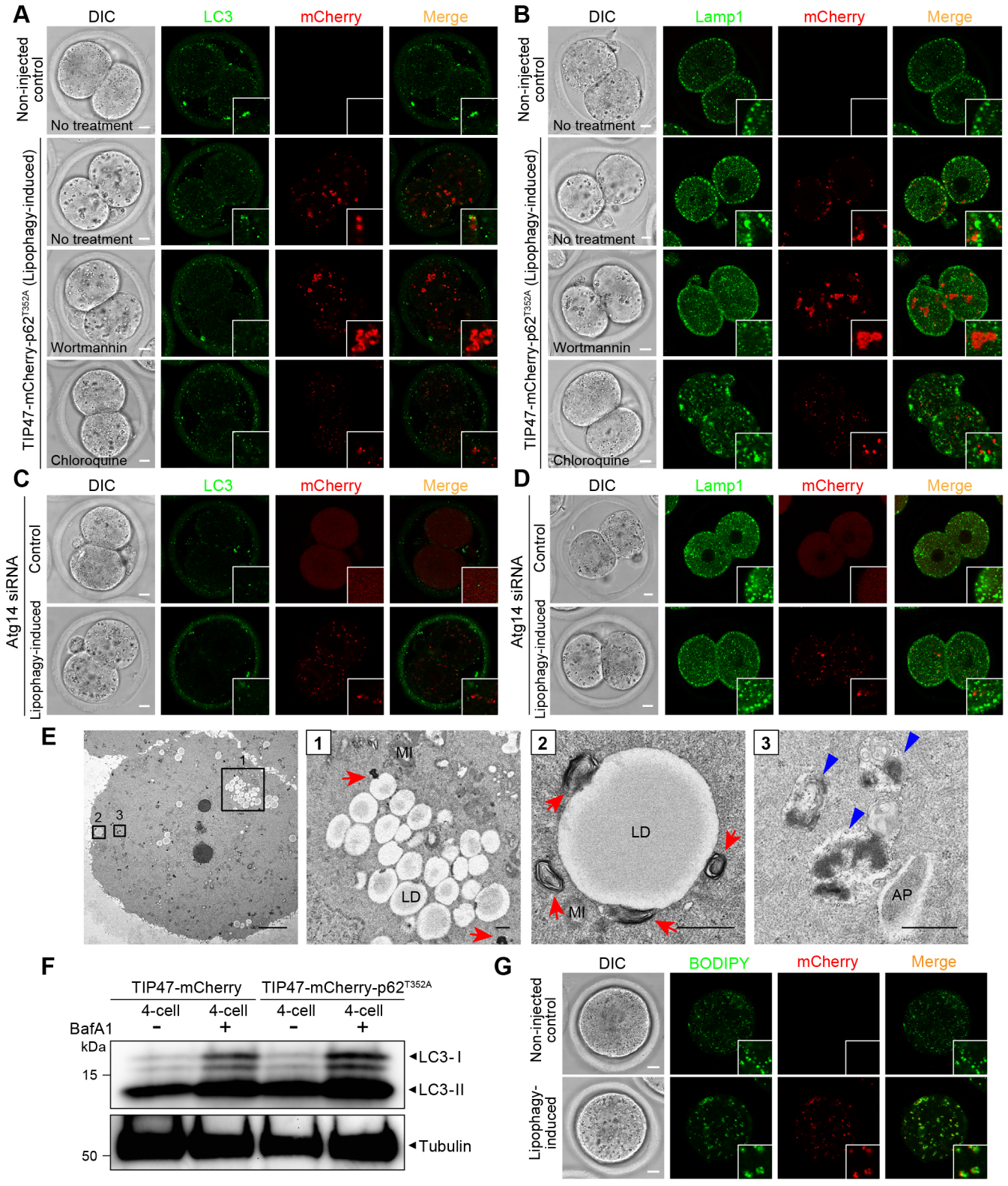

Fig. 4. See next page for legend.

with siRNA targeting Atg14. In contrast, lysosomal inhibition by chloroquine treatment shifted lysosome localization, but caused neither LD clustering nor translocation in lipophagy-induced embryos, indicating that lysosomal positioning influences the association between clustered LDs and lysosomes.

Unexpectedly, we found that forced lipophagy induction decreased embryonic viability (Fig. 5A,B), suggesting that LDs consumed by forced lipophagy at an early stage of embryonic development might be necessary at a later stage. Thus, preimplantation embryonic development requires not only endogenous lipolysis, but also the

Development (2018) 145, dev161893. doi:10.1242/dev.161893

Fig. 4. Forced lipophagy depends on autophagy.
(A,B) Immunofluorescence imaging of LD localization with LC3 (autophagosomes) or Lamp1 (lysosomes) in two-cell embryos injected with TIP47-mCherry-p62^{T352A} mRNA (lipophagy-induced) or not injected (non-injected control), and then co-cultured in the presence or absence of wortmannin or chloroquine for 24 h. (C,D) Immunofluorescence analysis of LD localization with LC3 or Lamp1 in two-cell embryos simultaneously injected with siRNA targeting Atg14 and either TIP47-mCherry (control) or TIP47-mCherry-p62^{T352A} mRNA (lipophagy-induced). (E) Electron microscopy images of lipophagy-induced embryos at the four-cell stage. Right three panels show higher-magnification images of the representative boxed areas (1, 2 and 3) in the left panel. Red arrows and blue arrowheads indicate lysosome and autolysosome, respectively. AP, autophagosome; LD, lipid droplet; MI, mitochondria. (F) Autophagic flux assay of embryos microinjected with TIP47-mCherry or TIP47-mCherry-p62^{T352A} mRNA. Embryos were co-cultured in the absence or presence of bafilomycin A_1 ($BafA_1$), and total cell extracts (70 embryos per lane) were subjected to immunoblot analysis using anti-LC3 antibody. The membrane was re-probed with anti-tubulin antibody as a loading control. (G) Unfertilized (MII) oocytes microinjected with or without TIP47-mCherry-p62^{T352A} mRNA were cultured for 2 days *in vitro*, stained with BODIPY 493/503, and observed by laser confocal fluorescence microscopy. DIC, differential interference contrast. Insets show higher-magnification images. Scale bars: 10 µm (A-D,G); 5 µm (E, left panel); 0.5 µm (E, right three panels).

proper amount of LDs. On the other hand, the developmental potential of lipophagy-induced embryos was not significantly influenced by the presence of amino acids. At present, we know little about the molecular machinery responsible for this phenomenon, but speculate that a signaling pathway that regulates autophagy [e.g. mammalian target of rapamycin (mTOR), which negatively regulates autophagy] or cellular energy balance [e.g. AMP-activated protein kinase (AMPK), which is activated by ATP depletion] could be involved, facilitating the recycling of fatty acids (FAs) generated by forced lipophagy.

By contrast, some lipophagy-induced embryos survived under conditions in which excess LDs accumulated (i.e. in the presence of OA and a lipase inhibitor) or lipotoxic species were generated (i.e. under PA supplementation). This result indicates that forced lipophagy attenuates lipotoxicity by eliminating excess LDs. Although the precise mechanism underlying tolerance of lipotoxicity remains unknown, it is possible that unsaturated FAs generated by forced lipophagy protect the cells against lipotoxic FAs, such as PA, as previously demonstrated in cultured mammalian cells (Listenberger et al., 2003). Further analysis will be required to determine whether tolerance of lipotoxicity is related to apoptosis.

An unresolved issue, based on our observations in mouse early embryos, is that TIP47-mCherry, used as an LD marker, did not work as expected. In contrast to the lipophagy-induced embryos (microinjected with TIP47-mCherry-p62^{T352A}), in which fluorescence was specifically detected at the LD surface, TIP47-mCherry-injected embryos exhibited diffuse fluorescence (Fig. S1C). Because post-translational modification of Plins, including phosphorylation and ubiquitylation, are involved in stabilizing the LD localization of these proteins (Orlicky et al., 2008; Xu et al., 2005), we speculated that some modification occurs at the C terminus of TIP47, which might affect its LD localization. Therefore, we created mCherry-TIP47 (C-terminally mCherry-tagged TIP47) and repeatedly microinjected it into one-cell embryos. However, although the new fusion protein was expressed, fluorescence signals were not detected at the LD surface, but instead remained diffusely distributed in the cytoplasm (Fig. S1D). On the other hand, mRNAs encoding either TIP47-mCherry-p62^{T352A} or mCherry-TIP47-p62^{T352A} could induce lipophagy, with the mCherry signals localized specifically at clustered LDs (Fig. S1C,D), indicating that p62 expression at the LD surface might stabilize TIP47 or its interaction with LDs. Because a previous study in cultured mammalian cells showed that TIP47 fails to associate with LD when full-length ADRP is simultaneously overexpressed, but not when an N-terminally modified (mutant or GFP-tagged) ADRP is overexpressed (Orlicky et al., 2008), we speculate that access of TIP47 to LDs is dependent on the level of ADRP. Consistent with this idea, ADRP is abundant in mouse oocytes and embryos (T.T. and S.T., unpublished). Our ongoing research using ADRP KO mice should be able to determine why TIP47 protein fused to either the N or C terminus of mCherry does not function as an LD marker in fertilized mouse embryos.

Cellular lipid content varies between animal species, probably because of differences in ATP requirements between oocyte maturation and subsequent embryonic development (Dunning et al., 2014). For example, in comparison with mouse and human, porcine oocytes contain massive amounts of LDs [37.3 ng fat/nl volume of oocyte in pig, versus 6.25 ng fat/nl in mouse (Leese, 2012)], which can negatively influence embryonic manipulation, especially in the case of cryopreservation (Nagashima et al., 1995). Because autophagy is highly conserved across animal species, it would be interesting to investigate the consequences of forced lipophagy in porcine embryos.

In summary, we achieved forced selective autophagy by expressing a p62 fusion protein, thereby generating cells depleted of a specific organelle. Using this system, we revealed that the correct amount of LDs is important for early embryonic development. The same strategy could be applied to generate other organelle-depleted cells to remove unwanted organelles and thus analyze organelle functions. Therefore, this method represents a valuable tool for elucidating the roles of specific organelles.

MATERIALS AND METHODS

Plasmid construction

To generate pCW TIP47-mCherry and pCW TIP47-mCherry-p62^{T352A}, TIP47 (1-221 amino acids) and human p62^{T352A} cDNA were cloned into pCW57.1 (Addgene plasmid #41393, deposited by David Root) along with mCherry. The plasmid DsRed-p62^{WT} was a kind gift from Dr Masaaki Komatsu (Niigata University, Japan).

Cell culture

HeLa cells were cultured in Dulbecco's Modified Eagle's medium (DMEM, Nacalai Tesque) supplemented with 10% fetal bovine serum (FBS, Biosera), 50 mg/ml penicillin, and streptomycin (regular medium) in a 5% CO_2 incubator. Atg14 KO HeLa cells were generated by clustered regularly interspaced short palindromic repeat (CRISPR) using pX459 GFP carrying the sgRNA expression cassette to target Atg14 (CAGAGGCATAATCG-CAAACT) as previously described (Takayama et al., 2017). TIP47-mCherry and TIP47-mCherry-p62^{T352A} cells were generated by lentiviral transduction with pCW, psPAX2 (Addgene plasmid #12260, deposited by Didier Trono) and pCMV VSV-G (Addgene plasmid #8454, deposited by Bob Weinberg). The stable cell lines were cultured in regular media containing 1 mg/ml doxycycline. For drug treatment, cells were incubated for the indicated times in medium containing 0.5 mM OA (Sigma-Aldrich). For LD staining, cells were cultured for 30 min in the presence of 1 µg/ml BODIPY 493/503 (Thermo Fisher Scientific).

Flow cytometry

Trypsinized cells were incubated with 1 µg/ml BODIPY 493/503 (Thermo Fisher Scientific) in PBS for 30 min at 4°C, and then sedimented by centrifugation at 5000 rpm (2500 ***g***) for 2 min. The pelleted cells were washed with PBS and then re-suspended in PBS containing 10% FBS and 1 µg/ml 4′,6-diamidino-2-phenylindole (DAPI), passed through a 70-µm cell strainer, and subjected to flow cytometry on a CytoFLEX S flow

Development (2018) 145, dev161893. doi:10.1242/dev.161893

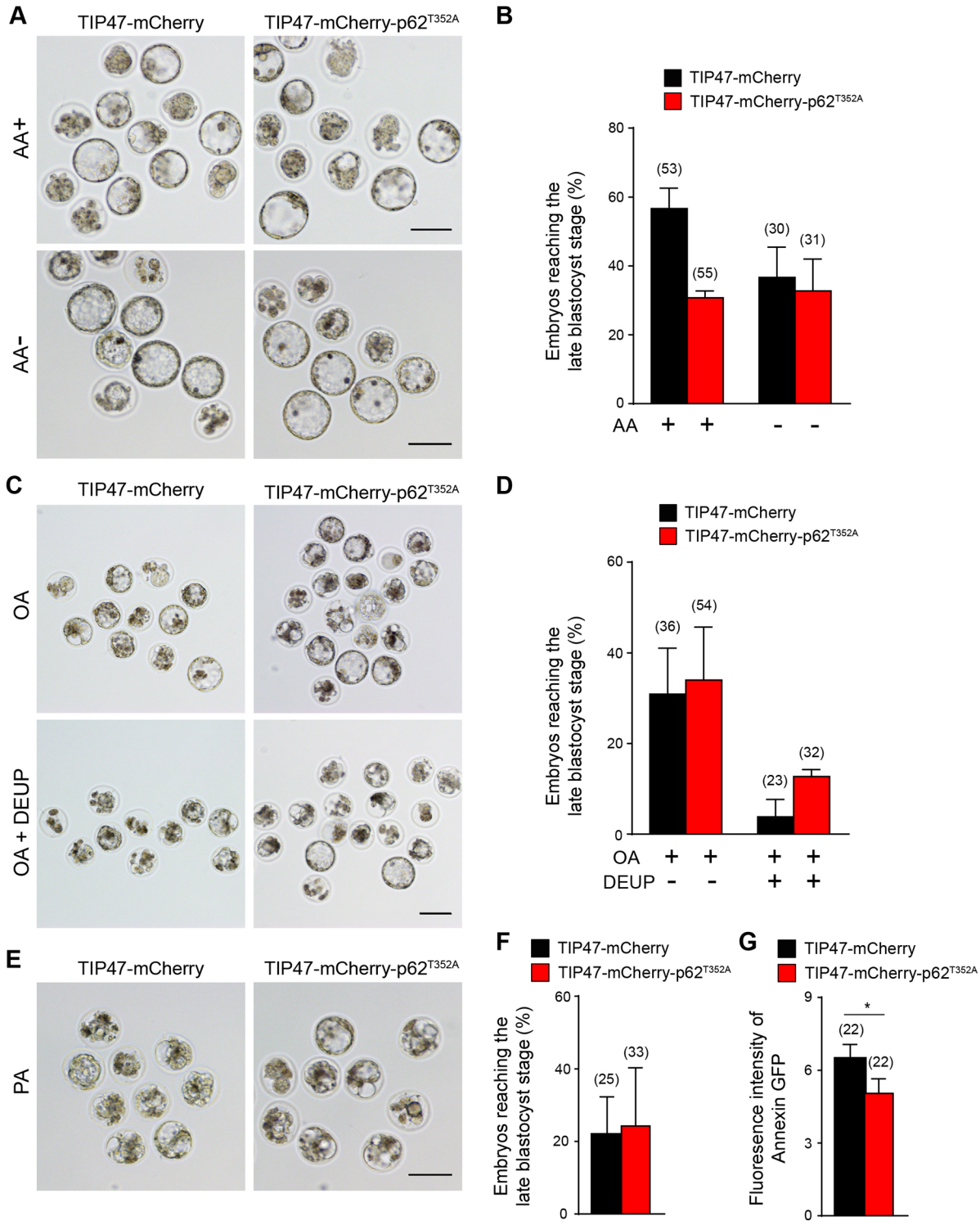

Fig. 5. See next page for legend.

cytometer equipped with NUV 375 nm (for DAPI), 488 nm (for GFP) and 561 nm (for mCherry) lasers (Beckman Coulter). Dead cells were detected by DAPI staining.

Mice and embryo manipulation

All mouse experiments were performed in accordance with the relevant guidelines and were approved by the Animal Care and Use Committee of the National Institute of Quantum and Radiological Science and Technology. Mice used in this study were 8- to 12-week-old C57BL/6J mice (Japan SLC), except for C3H mice (Japan SLC) used for the experiment described in Fig. S1B. Mice were housed under specific pathogen-free conditions. Metaphase II (MII) oocyte collection from superovulated females, embryo manipulation, *in vitro* fertilization, microinjection, and live-cell imaging were performed based on previously described methods (Kaizuka et al., 2016; Tsukamoto et al., 2014, 2013). For assessment of blastocysts, one-cell embryos were cultured for 4-5 days *in vitro*, and blastocyst formation was evaluated based on expansion of the blastocoel. We confirmed that 70% of control embryos (70.1±6.2%; from three independent experiments) injected

Development (2018) 145, dev161893. doi:10.1242/dev.161893

Fig. 5. Developmental potential of lipophagy-induced embryos.
(A) Representative images of embryos microinjected with TIP47-mCherry (control) or TIP47-mCherry-p62^{T352A} mRNA (lipophagy-induced) and cultured with or without amino acids (AA) until the blastocyst stage (96 h after IVF). (B) Percentage of control or lipophagy-induced embryos cultured with or without amino acids (AA) that reached the late blastocyst stage. (C) Representative images of embryos expressing TIP47-mCherry (control) or TIP47-mCherry-p62^{T352A} (lipophagy-induced) after 120 h of culture under the indicated conditions. (D) Percentage of control or lipophagy-induced embryos that reached the late blastocyst stage under the indicated culture conditions. (E) Representative images of embryos expressing TIP47-mCherry (control) or TIP47-mCherry-p62^{T352A} (lipophagy-induced) after 120 h of culture in the presence of PA. (F) Percentage of control or lipophagy-induced embryos that reached the late blastocyst stage when co-cultured with PA. (G) Intracellular level of apoptosis in control and lipophagy-induced embryos. Embryos expressing TIP47-mCherry or TIP47-mCherry-p62^{T352A}, cultured with PA to the blastocyst stage, were stained with Annexin V-EGFP, and total cellular fluorescence was measured by CCM. Error bars represent s.e.m.; numbers in parentheses indicate total number of embryos analyzed from three independent experiments; *P<0.05 (Student's t-test). Scale bars: 100 µm.

with TIP47-mCherry mRNA developed to early and growing blastocysts with a cavity volume greater than half the volume of the embryo. We considered developing embryos with cavities that completely filled the embryo as late blastocysts. When necessary, embryos were cultured with KSOM lacking amino acids (Eagle's essential and non-essential amino acids), and glutamine. In some experiments, one-cell embryos were cultured with the following chemicals: 200 nM $BafA_1$ (WAKO Pure Chemical Industries), 100 µM DEUP (Sigma-Aldrich), 0.1 mM OA, 0.1 mM PA (Sigma-Aldrich), 10 µM wortmannin (Sigma-Aldrich) or 50 µM chloroquine (WAKO Pure Chemical Industries).

For RNAi experiments, Stealth RNAi duplex oligonucleotides (siRNAs) were designed to target Atg3 (MSS228710, Invitrogen) or Atg14 (MSS211913, Invitrogen). Stealth RNAi Negative Control Duplexes (Invitrogen) were used as negative controls. Knockdown efficiency was calculated based on conversion of LC3-I to LC3-II, as determined by immunoblot analysis (Fig. S2B), as well as by immunofluorescence analysis of LC3 (Fig. 4C). In addition, we assessed whether embryos injected with siRNAs were developmentally compromised (Fig. S2A), based on our previous observation that autophagy-deficient embryos (derived from oocyte-specific *Atg5* knockout females) die before implantation (Tsukamoto et al., 2008). Based on these analyses, we chose siRNA targeting Atg14, which inhibited development more efficiently than siRNA against Atg3, for further study.

In vitro transcription and RNA microinjection

In vitro transcription and microinjection were performed as described (Tsukamoto et al., 2014). Briefly, plasmids encoding the indicated mRNAs were linearized, and capped mRNAs with poly (A) tailing were synthesized using the mMESSAGE mMACHINE Ultra Kit (Ambion). The purified mRNAs were diluted to 100 ng/µl in TE buffer, filtered, and microinjected into the cytoplasm of oocytes or embryos. For the RNAi experiment, 10 µM siRNA was microinjected simultaneously with either TIP47-mCherry or TIP47-mCherry-p62^{T352A} mRNA into the cytoplasm of fertilized embryos, as described above, except that these mixtures were not filtered before microinjection.

Fluorescence microscopy

Cells expressing fluorescently tagged protein were grown on coverslips and fixed in 3.7% formaldehyde in PBS for 15 min. For LD staining, the fixed cells were incubated with 1 µg/ml BODIPY 493/503 in PBS for 30 min and observed under a confocal laser microscope (FV1000 IX81, Tokyo, Japan) using a 60× oil-immersion objective lens with a numerical aperture (NA) of 1.42.

Immunofluorescence of mouse embryos was performed as previously described (Tsukamoto et al., 2014). Briefly, fixed embryos were blocked and permeabilized overnight at 4°C with 0.4% Triton X-100 in PBS containing 10% goat serum and 3% bovine serum albumin (BSA). The permeabilized embryos were then incubated with the following primary antibodies, diluted in PBS containing 3% BSA (PBS/BSA), overnight at 4°C: anti-LC3B (Cosmo Bio; CAC-CTB-LC3-2-IC; 1:200), anti-Lamp1 (Abcam; ab25245; 1:200), anti-ubiquitin (Medial & Biological Laboratories; D058-3; 1:200) and anti-Atp5a (Abcam; ab14748; 1:200). The embryos were washed in PBS/BSA at least four times for 15 min each, and then incubated with the appropriate secondary antibodies (1:800) for 1 h at room temperature or overnight at 4°C. Embryos were then washed once more, and transferred to PBS/BSA in a glass-bottomed dish (Matsunami Glass) covered with mineral oil. Fluorescence images were acquired with a SP8 laser scanning confocal system (Leica, TCS, SP8) with a 63× Plan APO 1.4 NA oil immersion objective.

For labeling of LDs, fixed oocytes or embryos were stained with BODIPY 493/503 solution (1 µg/ml, diluted in PBS/BSA) in the dark for 10-15 min at room temperature, washed several times with PBS/BSA, and observed by laser confocal microscopy as described above. Fluorescence measurements were performed using ImageJ software (NIH). Images were adjusted in Photoshop and Illustrator (Adobe).

To measure ROS production, embryos were incubated with 10 µM aminophenyl fluorescein (APF, GORYO Chemical) for 30 min in PBS containing polyvinylpyrrolidone (PVP, Sigma-Aldrich) instead of BSA to avoid interference with fluorescence measurements. Fluorescence was imaged on a real-time cultured cell monitoring system (CCM, ASTEC Co.) with a 10× objective lens (Plan, NA0.25, Nikon), and analyzed using ImageJ software as described before.

To monitor cellular apoptosis, embryos were stained using the Annexin V-EGFP Apoptosis Kit (BioVision, #K104-25), which includes Annexin V-EGFP and propidium iodide. Fluorescence was analyzed by CCM, and fluorescence measurements were performed as described above.

Immunoblotting

Immunoblotting was performed based on previously described methods (Tsukamoto et al., 2014). The following antibodies were used: anti-LC3B (Cell Signaling Technology; #12741; 1:400) and anti-α/β-tubulin (Cell Signaling Technology; #2148; 1:500). Horseradish peroxidase (HRP)-conjugated anti-mouse and anti-rabbit IgG antibodies were purchased from Cell Signaling Technology (#7076 and #7074, respectively). For the autophagic flux assay, immunoblots were performed according to previously reported guidelines for monitoring autophagy (Klionsky et al., 2016). Briefly, 70 control or lipophagy-induced embryos were cultured in the absence or presence of $BafA_1$ and lysed for immunoblotting. After SDS-PAGE, proteins were blotted onto PVDF membrane using a Trans-Blot Turbo Transfer System (Bio-Rad). The blots were blocked with 3% BSA in TBS-T (Bio-Rad) for 1 h, and then incubated with primary antibodies at 4°C overnight. Subsequently, the membranes were washed three times for 10 min each with TBS-T (Bio-Rad), and then incubated with the appropriate HRP-conjugated secondary antibodies as described above. The signals were visualized using a SuperSignal West Femto Chemiluminescent Substrate (Thermo Fisher) and imaged on a ChemiDoc system (UVP).

Electron microscopy

Electron microscopy was performed as described previously (Tsukamoto et al., 2013). LD number and size were quantified using the ImageJ segmentation tool (NIH).

TG measurement

For TG measurements, 40 embryos per experiment were transferred into 10 µl of water (Nippon Gene) and stored at −80°C until use. TG levels were assayed using the Picoprobe Triglyceride Fluorometric Assay kit (BioVision, #K614-100). In this assay, TG is converted to glycerol and FA, and the resultant glycerol is oxidized to generate a product that reacts with the picoprobe and developer (included in the kit) to generate fluorescence. Because the resultant fluorescence is directly proportional to the amount of TG, TG content was quantitated by fluorometry. The fluorescence was measured on a QFX Fluorometer (DeNovix), and TG level was calculated using a standard curve.

ATP measurement

Intracellular ATP levels were determined using the IntraCellular ATP assay kit (TOYO B-Net Co.). In brief, embryos cultured to the indicated stage were

individually transferred into 100 µl of water, and then mixed with 100 µl of the kit reaction buffer, followed by incubation for 10 min at room temperature. ATP was measured immediately using a GENELIGHT (Microtec Co., #GL-220A). ATP content was calculated using a standard curve, prepared using the ATP provided with the kit.

Statistics

Data were compared using unpaired Student's *t*-test in Prism 6 (GraphPad). Statistical significance is represented as $*P<0.05$, unless otherwise stated.

Acknowledgements

We thank Dr Noboru Mizushima (The University of Tokyo) for his mentorship and encouragement. We also thank Masaaki Komatsu (Niigata University) for providing the DsRed-p62^{WT} plasmid, and Ayako Wada and Tomomi Hatakeyama for technical assistance.

Competing interests

The authors declare no competing or financial interests.

Author contributions

Conceptualization: T.T., E.I., S.T.; Methodology: T.T., K.T., S.I., E.I., S.T.; Investigation: T.T., K.T., S.I., A.Y., E.I., S.T.; Data curation: T.T., S.I., A.Y., T.H., N. Minami, N. Miyasaka, T.K., A.M., E.I., S.T.; Writing - original draft: T.T., E.I., S.T.; Writing - review & editing: T.H., N. Minami, N. Miyasaka, T.K., A.M., E.I., S.T.; Supervision: E.I., S.T.; Project administration: E.I., S.T.; Funding acquisition: E.I., S.T.

Funding

This work was supported by Japan Society for the Promotion of Science (KAKENHI Program; 16H06167 and 16H01194 to E.I.; 25111001 and 15H05637 to S.T.), Japan Agency for Medical Research and Development (16gk0110015h0001 to T.T. and S.T.), the Naito Foundation (to E.I.), the Senri Life Science Foundation (to E.I.) and the Takeda Science Foundation (to E.I. and S.T.).

Supplementary information

Supplementary information available online at
http://dev.biologists.org/lookup/doi/10.1242/dev.161893.supplemental

References

Anding, A. L. and Baehrecke, E. H. (2017). Cleaning house: selective autophagy of organelles. *Dev. Cell* **41**, 10-22.

Bickel, P. E., Tansey, J. T. and Welte, M. A. (2009). PAT proteins, an ancient family of lipid droplet proteins that regulate cellular lipid stores. *Biochim. Biophys. Acta* **1791**, 419-440.

Bradley, J., Pope, I., Masia, F., Sanusi, R., Langbein, W., Swann, K. and Borri, P. (2016). Quantitative imaging of lipids in live mouse oocytes and early embryos using CARS microscopy. *Development* **143**, 2238-2247.

Bulankina, A. V., Deggerich, A., Wenzel, D., Mutenda, K., Wittmann, J. G., Rudolph, M. G., Burger, K. N. J. and Höning, S. (2009). TIP47 functions in the biogenesis of lipid droplets. *J. Cell Biol.* **185**, 641-655.

Dunning, K. R., Russell, D. L. and Robker, R. L. (2014). Lipids and oocyte developmental competence: the role of fatty acids and beta-oxidation. *Reproduction* **148**, R15-R27.

Fujimoto, T. and Parton, R. G. (2011). Not just fat: the structure and function of the lipid droplet. *Cold Spring Harb. Perspect. Biol.* **3**, a004838.

Herms, A., Bosch, M., Reddy, B. J. N., Schieber, N. L., Fajardo, A., Rupérez, C., Fernández-Vidal, A., Ferguson, C., Rentero, C., Tebar, F. et al. (2015). AMPK activation promotes lipid droplet dispersion on detyrosinated microtubules to increase mitochondrial fatty acid oxidation. *Nat. Commun.* **6**, 7176.

Ichimura, Y., Kumanomidou, T., Sou, Y.-S., Mizushima, T., Ezaki, J., Ueno, T., Kominami, E., Yamane, T., Tanaka, K. and Komatsu, M. (2008). Structural basis for sorting mechanism of p62 in selective autophagy. *J. Biol. Chem.* **283**, 22847-22857.

Itakura, E., Kishi, C., Inoue, K. and Mizushima, N. (2008). Beclin 1 forms two distinct phosphatidylinositol 3-kinase complexes with mammalian Atg14 and UVRAG. *Mol. Biol. Cell* **19**, 5360-5372.

Kaizuka, T., Morishita, H., Hama, Y., Tsukamoto, S., Matsui, T., Toyota, Y., Kodama, A., Ishihara, T., Mizushima, T. and Mizushima, N. (2016). An autophagic flux probe that releases an internal control. *Mol. Cell* **64**, 835-849.

Katsuragi, Y., Ichimura, Y. and Komatsu, M. (2015). p62/SQSTM1 functions as a signaling hub and an autophagy adaptor. *FEBS J.* **282**, 4672-4678.

Kaushik, S. and Cuervo, A. M. (2015). Degradation of lipid droplet-associated proteins by chaperone-mediated autophagy facilitates lipolysis. *Nat. Cell Biol.* **17**, 759-770.

Klionsky, D. J., Abdelmohsen, K., Abe, A., Abedin, M. J., Abeliovich, H., Acevedo Arozena, A., Adachi, H., Adams, C. M., Adams, P. D., Adeli, K. et al. (2016). Guidelines for the use and interpretation of assays for monitoring autophagy (3rd edition). *Autophagy* **12**, 1-222.

Komatsu, M., Kurokawa, H., Waguri, S., Taguchi, K., Kobayashi, A., Ichimura, Y., Sou, Y. S., Ueno, I., Sakamoto, A., Tong, K. I. et al. (2010). The selective autophagy substrate p62 activates the stress responsive transcription factor Nrf2 through inactivation of Keap1. *Nat. Cell Biol.* **12**, 213-223.

Kory, N., Thiam, A.-R., Farese, R. V., Jr and Walther, T. C. (2015). Protein crowding is a determinant of lipid droplet protein composition. *Dev. Cell* **34**, 351-363.

Leese, H. J. (2012). Metabolism of the preimplantation embryo: 40 years on. *Reproduction* **143**, 417-427.

Listenberger, L. L., Han, X., Lewis, S. E., Cases, S., Farese, R. V., Jr, Ory, D. S. and Schaffer, J. E. (2003). Triglyceride accumulation protects against fatty acid-induced lipotoxicity. *Proc. Natl. Acad. Sci. USA* **100**, 3077-3082.

Martinez-Lopez, N., Garcia-Macia, M., Sahu, S., Athonvarangkul, D., Liebling, E., Merlo, P., Cecconi, F., Schwartz, G. J. and Singh, R. (2016). Autophagy in the CNS and periphery coordinate lipophagy and lipolysis in the brown adipose tissue and liver. *Cell Metab.* **23**, 113-127.

Mizushima, N. (2007). Autophagy: process and function. *Genes Dev.* **21**, 2861-2873.

Nagashima, H., Kashiwazaki, N., Ashman, R. J., Grupen, C. G. and Nottle, M. B. (1995). Cryopreservation of porcine embryos. *Nature* **374**, 416.

Okamoto, K. (2014). Organellophagy: eliminating cellular building blocks via selective autophagy. *J. Cell Biol.* **205**, 435-445.

Orlicky, D. J., Degala, G., Greenwood, C., Bales, E. S., Russell, T. D. and McManaman, J. L. (2008). Multiple functions encoded by the N-terminal PAT domain of adipophilin. *J. Cell Sci.* **121**, 2921-2929.

O'Rourke, E. J. and Ruvkun, G. (2013). MXL-3 and HLH-30 transcriptionally link lipolysis and autophagy to nutrient availability. *Nat. Cell Biol.* **15**, 668-676.

Pankiv, S., Clausen, T. H., Lamark, T., Brech, A., Bruun, J.-A., Outzen, H., Øvervatn, A., Bjørkøy, G. and Johansen, T. (2007). p62/SQSTM1 binds directly to Atg8/LC3 to facilitate degradation of ubiquitinated protein aggregates by autophagy. *J. Biol. Chem.* **282**, 24131-24145.

Rodriguez, A., Durán, A., Selloum, M., Champy, M.-F., Diez-Guerra, F. J., Flores, J. M., Serrano, M., Auwerx, J., Diaz-Meco, M. T. and Moscat, J. (2006). Mature-onset obesity and insulin resistance in mice deficient in the signaling adapter p62. *Cell Metab.* **3**, 211-222.

Singh, R., Kaushik, S., Wang, Y., Xiang, Y., Novak, I., Komatsu, M., Tanaka, K., Cuervo, A. M. and Czaja, M. J. (2009). Autophagy regulates lipid metabolism. *Nature* **458**, 1131-1135.

Stolz, A., Ernst, A. and Dikic, I. (2014). Cargo recognition and trafficking in selective autophagy. *Nat. Cell Biol.* **16**, 495-501.

Sturmey, R. G., Reis, A., Leese, H. J. and McEvoy, T. G. (2009). Role of fatty acids in energy provision during oocyte maturation and early embryo development. *Reprod. Domest. Anim.* **44** Suppl. 3, 50-58.

Takayama, K., Matsuura, A. and Itakura, E. (2017). Dissection of ubiquitinated protein degradation by basal autophagy. *FEBS Lett.* **591**, 1199-1211.

Thiam, A. R., Farese, R. V., Jr and Walther, T. C. (2013). The biophysics and cell biology of lipid droplets. *Nat. Rev. Mol. Cell Biol.* **14**, 775-786.

Tsukamoto, S., Kuma, A., Murakami, M., Kishi, C., Yamamoto, A. and Mizushima, N. (2008). Autophagy is essential for preimplantation development of mouse embryos. *Science* **321**, 117-120.

Tsukamoto, S., Hara, T., Yamamoto, A., Ohta, Y., Wada, A., Ishida, Y., Kito, S., Nishikawa, T., Minami, N., Sato, K. et al. (2013). Functional analysis of lysosomes during mouse preimplantation embryo development. *J. Reprod. Dev.* **59**, 33-39.

Tsukamoto, S., Hara, T., Yamamoto, A., Kito, S., Minami, N., Kubota, T., Sato, K. and Kokubo, T. (2014). Fluorescence-based visualization of autophagic activity predicts mouse embryo viability. *Sci. Rep.* **4**, 4533.

Walther, T. C. and Farese, R. V.Jr. (2012). Lipid droplets and cellular lipid metabolism. *Annu. Rev. Biochem.* **81**, 687-714.

Wang, C.-W., Miao, Y.-H. and Chang, Y.-S. (2014). A sterol-enriched vacuolar microdomain mediates stationary phase lipophagy in budding yeast. *J. Cell Biol.* **206**, 357-366.

Watanabe, T., Thayil, A., Jesacher, A., Grieve, K., Debarre, D., Wilson, T., Booth, M. and Srinivas, S. (2010). Characterisation of the dynamic behaviour of lipid droplets in the early mouse embryo using adaptive harmonic generation microscopy. *BMC Cell Biol.* **11**, 38.

Xu, G., Sztalryd, C., Lu, X., Tansey, J. T., Gan, J., Dorward, H., Kimmel, A. R. and Londos, C. (2005). Post-translational regulation of adipose differentiation-related protein by the ubiquitin/proteasome pathway. *J. Biol. Chem.* **280**, 42841-42847.

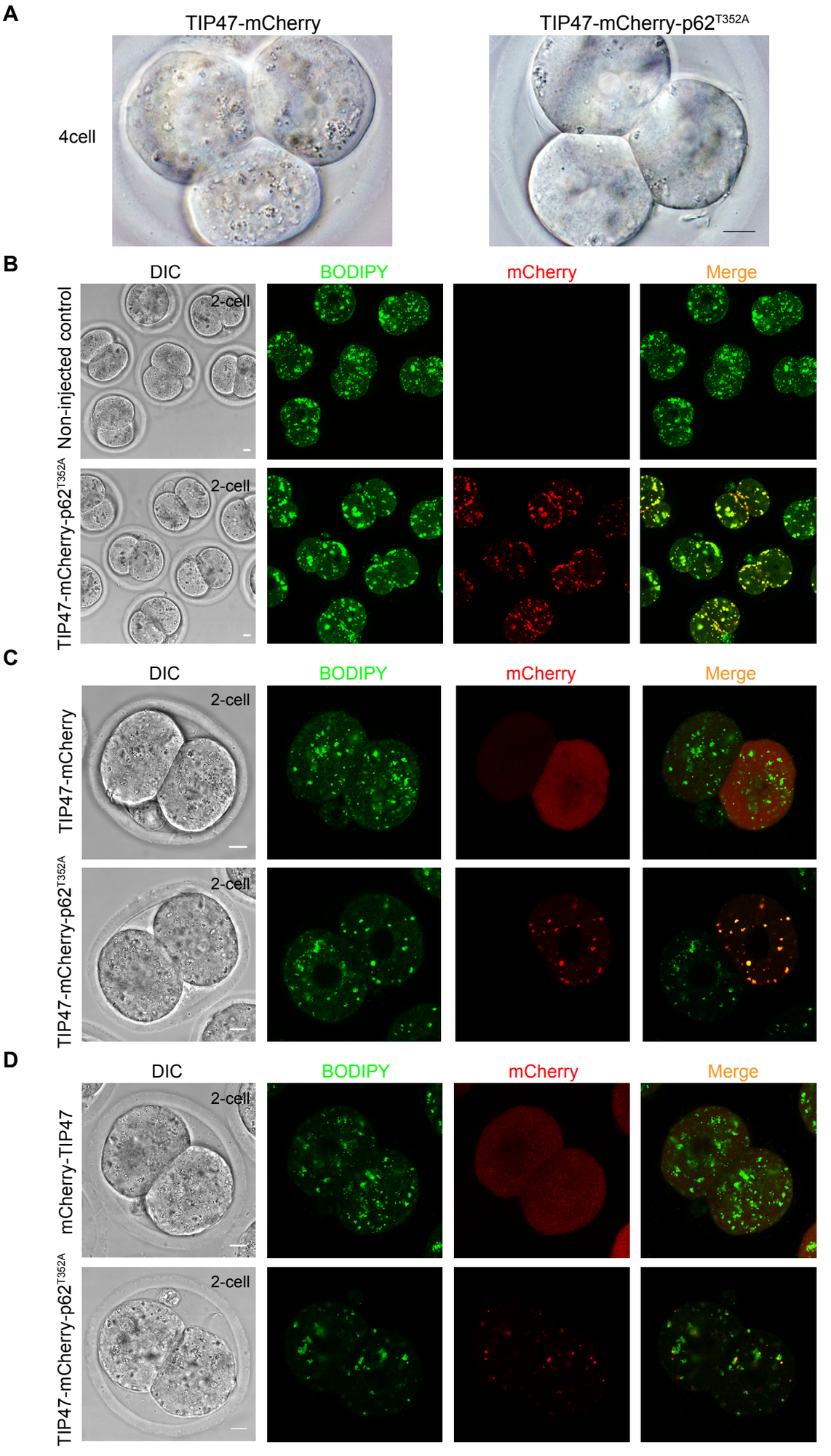

Fig. S1. Forced lipophagy in fertilized mouse embryos.

(A) Morphology of LDs in four-cell embryos expressing either TIP47-mCherry or TIP47-mCherry-p62^{T352A}. Scale bars, 10 μm.

(B) C3H mouse two-cell embryos, microinjected with or without TIP47-mCherry- p62^{T352A} mRNA, were stained with BODIPY 493/503 and observed by laser confocal fluorescence microscopy. DIC: differential interference contrast. Scale bars, 10 μm.

(C) mRNA for either TIP47-mCherry or TIP47-mCherry-p62^{T352A} was microinjected into one blastomere of two-cell embryos, which were then cultured for several hours, stained with BODIPY 493/503, and observed by laser confocal fluorescence microscopy.
DIC: differential interference contrast. Scale bars, 10 μm.

(D) Two-cell embryos microinjected at the one-cell stage with mRNA encoding either mCherry-TIP47 or mCherry-TIP47-p62^{T352A} (instead of TIP47-mCherry or TIP47-mCherry-p62^{T352A}) were stained with BODIPY 493/503 and observed by laser confocal fluorescence microscopy.
DIC: differential interference contrast. Scale bars, 10 μm.

Note that mRNAs for either TIP47-mCherry or mCherry-TIP47 were not detected at the LD surface, and instead remained diffusely distributed in the cytoplasm, whereas mRNAs encoding either TIP47-mCherry-p62^{T352A} or mCherry-TIP47-p62^{T352A} could induce lipophagy, suggesting that p62 expression at the LD surface stabilizes TIP47 or its interaction with LDs.

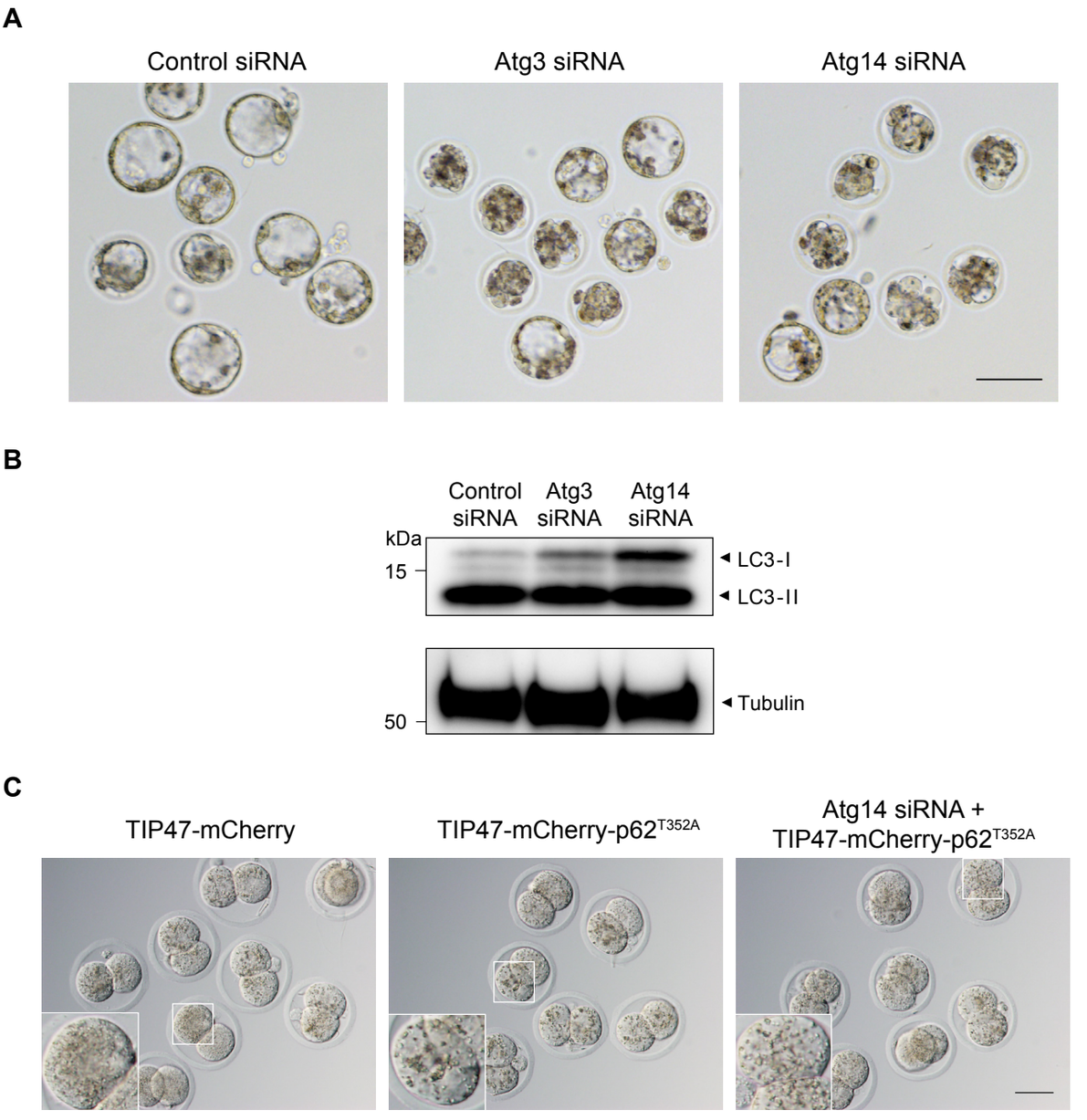

Fig. S2. Blocking of embryonic autophagic activity by siRNA injection.

(A) Representative images of embryos microinjected with control siRNA or siRNA targeting either Atg3 or Atg14, and cultured to the blastocyst stage. Scale bars, 100 µm.

(B) Immunoblotting of LC3 in embryos microinjected with control siRNA or siRNA targeting either Atg3 (Atg3 siRNA) or Atg14 (Atg14 siRNA), and cultured to the 8-cell stage. Total cell extracts (35 embryos per lane) were subjected to immunoblot analysis with anti-LC3 antibody. The membrane was re-probed with anti-tubulin antibody (as a loading control). Note that LC3 lipidation (LC3-II form) was detected even in Atg14 siRNA-injected embryos, even though autophagic activity was profoundly inhibited (Fig. 4C; LC3 dots [representing autophagosome] were almost absent in these embryos). A similar phenomenon was observed upon RNAi-mediated suppression of Atg14 in HeLa cells (Itakura et al., 2008), as well as in Atg14-deficient mouse embryonic fibroblasts (Matsunaga et al., 2009).

(C) Morphology of LDs in embryos microinjected with either TIP47-mCherry (left) or TIP47-mCherry-p62^{T352A} (middle) or a mixture of TIP47-mCherry-p62^{T352A} and Atg14 siRNA, and cultured to the 2-cell stage. Inset, higher-magnification image. Scale bars, 50 µm.

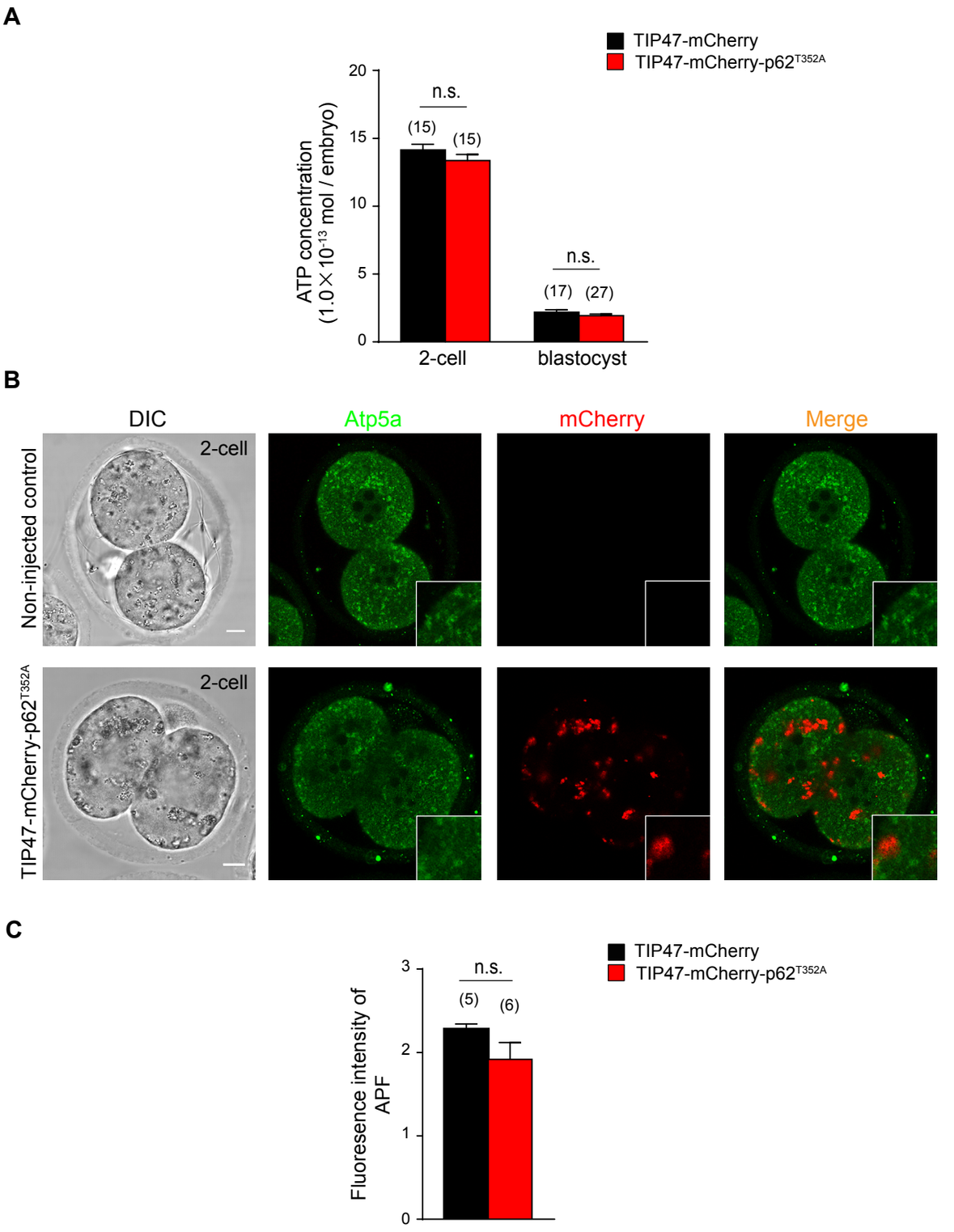

Fig. S3. Intracellular energy level does not change in lipophagy-induced embryos.

(A) ATP content of embryos expressing or not expressing TIP47-mCherry-p62^{T352A} was analyzed at the indicated stage. The number of embryos analyzed is shown above each error bar. Error bars, S.E.M.; n.s., not significant.

(B) Immunofluorescence imaging of LD colocalization with Atp5a (mitochondria marker) in two-cell embryos either injected or not injected with TIP47-mCherry-p62^{T352A} mRNA. Inset, higher-magnification image. Scale bars, 10 μm.

(C) ROS levels did not change between control and lipophagy-induced embryos. Embryos expressing either TIP47-mCherry or TIP47-mCherry-p62^{T352A} were cultured until the blastocyst stage, and then stained with aminophenyl fluorescein. Total cellular fluorescence was estimate by CCM. Error bars, S.E.M.; n.s., not significant.

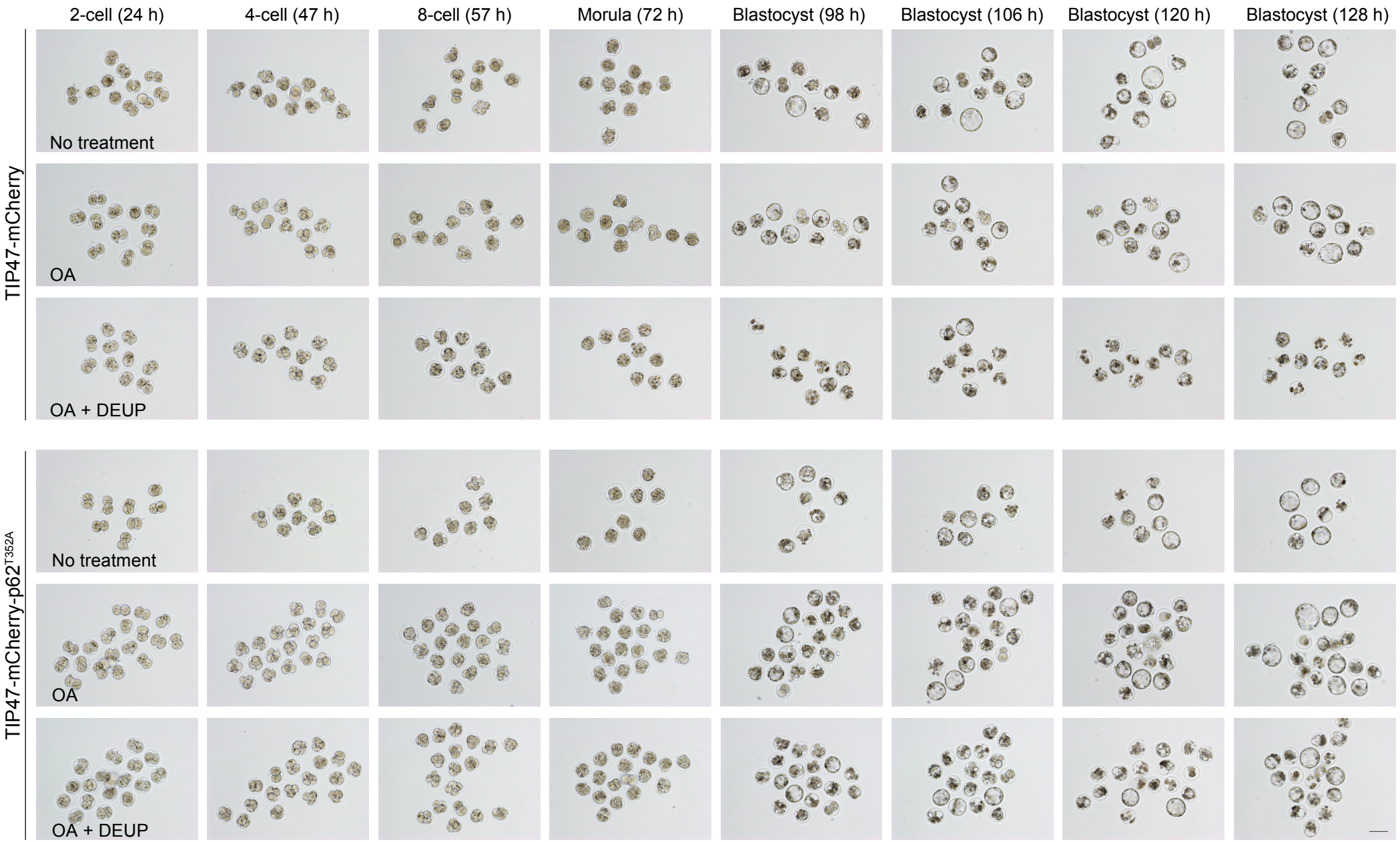

Fig. S4. Preimplantation development of lipophagy-induced embryos.

Representative examples of embryos expressing TIP47-mCherry or TIP47-mCherry-p62^{T352A}, cultured under the indicated conditions.
Parentheses, time after IVF. Scale bars, 100 μm.

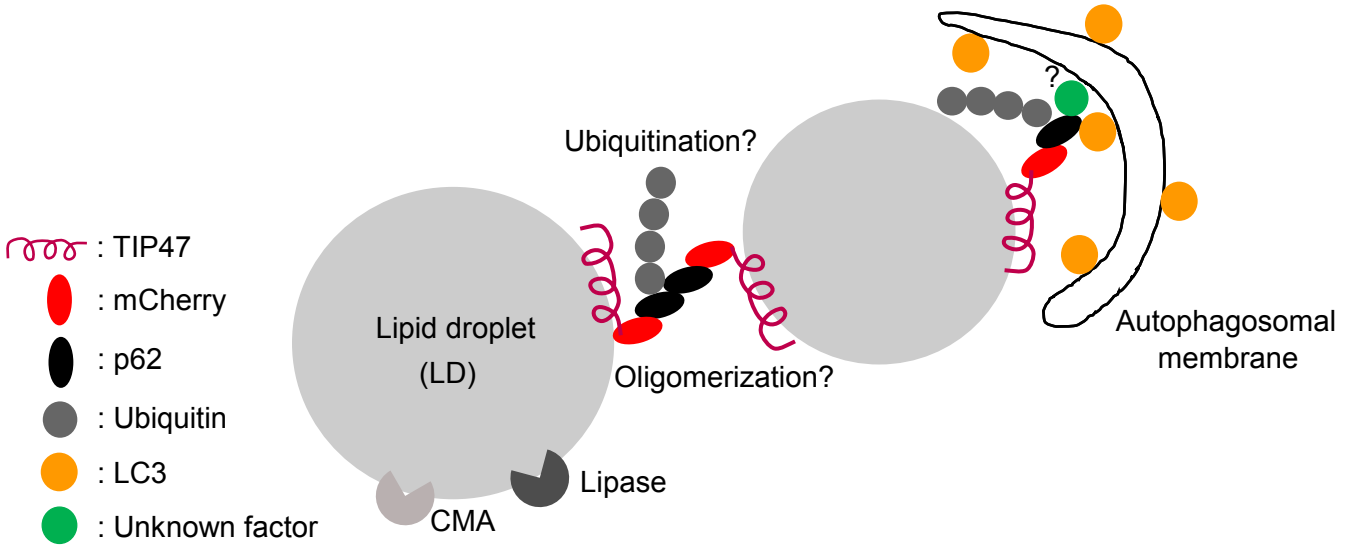

Fig. S5. Model of forced lipophagy.

p62 localized on the LD surface can interact with LC3. Because LC3 associates stably with autophagosomes, the fraction of LDs sequestered by the autophagosome is delivered to the lysosome for degradation. See details in the Discussion.

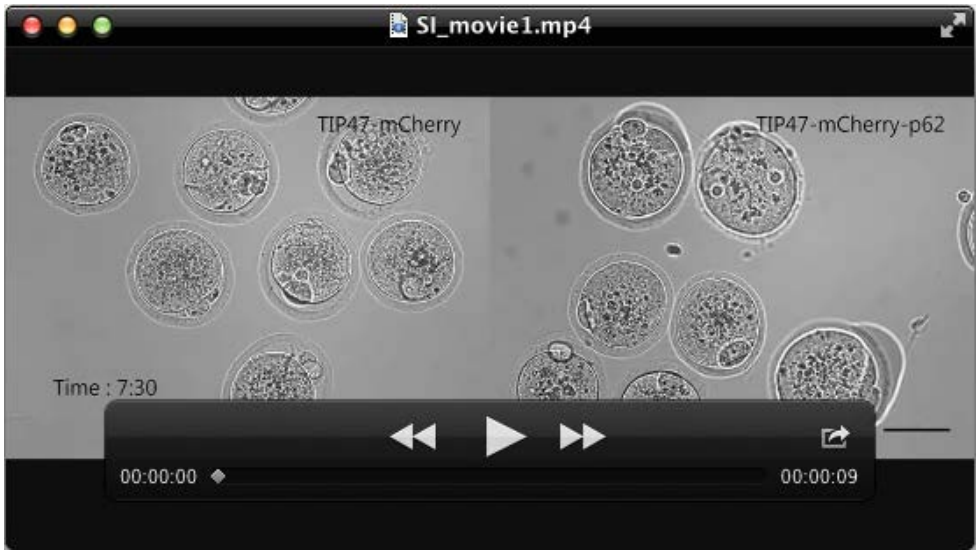

Movie 1. Morphology of LDs in lipophagy-induced embryos.

Live-cell imaging of developing mouse embryos injected with TIP47-mCherry (left) or TIP47-mCherry-p62 mRNA (right).
Time, post-IVF (hr:min). Scale bars, 100 µm. (mp4; 3.1 MB)

Supplemental references.

Itakura, E., Kishi, C., Inoue, K. and Mizushima, N. (2008). *Beclin 1 forms two distinct phosphatidylinositol 3-kinase complexes with mammalian Atg14 and UVRAG. Mol Biol Cell 19, 5360-5372.*

Matsunaga, K., Saitoh, T., Tabata, K., Omori, H., Satoh, T., Kurotori, N., Maejima, I., Shirahama-Noda, K., Ichimura, T., Isobe, T., et al. (2009). *Two Beclin 1-binding proteins, Atg14L and Rubicon, reciprocally regulate autophagy at different stages. Nature cell biology 11, 385-396.*